Structure and Dynamics of Silica-Filled Polymers by SANS and Coherent SAXS

Erik Geissler, Anne-Marie Hecht, Cyrille Rochas, Ferenc Horkay, Françoise Bley and Frédéric Livet*

Laboratoire de Spectrométrie Physique UMR CNRS 5588, Université J. Fourier de Grenoble, B.P.87, 38402 St Martin d'Hères Cedex, France

Laboratory of Integrative and Medical Biophysics, National Institutes of Health, 13 South Drive, Bethesda MD 20892, USA

Laboratoire de Thermodynamique et Physico-chimie Métallurgiques, CNRS UMR 4777, INPG, 38402 St Martin d'Hères Cedex, France

SUMMARY: Random crosslinking in elastomers gives birth to local variations in the crosslink density. When the network is swollen in a low-molecular-weight solvent, competition between the osmotic pressure and the local elastic constraints transforms these variations into differences in polymer concentration, the range and amplitude of which can be measured by small-angle X-ray or neutron scattering (SAXS or SANS). In filled systems, the distribution both of the polymer and of the elastic constraints is modified. By varying the proportion of deuterated solvent in the network, the scattering function of the polymer can be distinguished from that of the filler using SANS. Such measurements yield not only the internal surface area of the filler particles but also the fraction of that surface in contact with the polymer. The recently developed technique of quasi-elastic SAXS detects slow dynamic processes at wave vectors larger than those accessible with visible light lasers. This technique is used to investigate the dynamics of filler particles in uncrosslinked polymer melts. It is directly shown that the structural reorganization process of the filler following an external mechanical perturbation is diffusion-controlled.

Introduction

According to the scaling theory [1], thermodynamic properties of polymer solutions depend on a single characteristic length. Under the semidilute conditions, where different coils overlap, this distance is the thermal correlation length, ξ. When crosslinks are introduced into the polymer in a sufficient number to generate a network, the osmotic properties of the solution persist, but a new length scale Ξ is required to describe the elastic perturbations imposed by the crosslinks. In a dry rubber without solvent, neither of these length scales is directly visible. If, however, a low-molecular-weight solvent is introduced into the network, the resulting osmotic pressure is balanced by the local elastic pressure. As crosslinks are not uniformly distributed, random permanent local variations in concentration develop as the

 CCC 1022-1360/00/$ 17,50+.50/0

network swells, which scatter radiation. If filler particles are also present, the distribution of the polymer is modified. The characteristic lengths, which are generally significant in rubbers, typically range from 1 to 100 nm. This size range coincides with the optimum sensitivity of small-angle neutron or X-ray scattering (SANS or SAXS) [2]. Furthermore, by using mixtures of normal and deuterated polymers in the solvent, it is possible to discriminate between the signal from the polymer and that of the filler. The slow dynamics of the filler particles in the polymer matrix can be explored by means of X-ray correlation spectroscopy.

Experimental Part

Sample preparation

Linear vinyl-terminated poly(dimethylsiloxane) (viscosity 20 Pas) was blended with 9 % w/w of fumed silica filler. Two different fillers were used; the first was an untreated hydrophilic silica (AE300, Degussa, specific surface area 300 m^2g^{-1}, sample 1), and the other with octamethyltetrasiloxane grafted to its surface (AE60, Degussa, specific surface area 60 m^2g^{-1}, sample 2).

Both samples were prepared by mixing the filler and the polymer melt in a ball mill under dry nitrogen at 70 °C for 3 h. The resulting mixtures form thixotropic pastes that can be swollen in toluene. The measurements reported here were performed at polymer volume fraction $\varphi = 0.2$. The samples were swollen in mixtures of toluene (Prolabo, Analytical Grade) and deuterated toluene (Acros) with deuterium content > 99 %. The specimens for SANS were contained in a cell consisting of 1-mm thick quartz windows separated by a 1-mm-spacer sealed with a Viton O-ring.

Small-angle neutron scattering measurements

SANS measurements were made on the NG3 instrument at NIST, Gaithersburg, using an incident wavelength of $\lambda = 8$ Å and selector bandwidth $\Delta\lambda/\lambda = 10$ %. The detector was placed at three distances, 1.8 m, 6 m and 13.1 m from the sample. The range of wave vector q [= $(4\pi/\lambda)\sin\theta/2$, λ being the incident wavelength and θ the scattering angle] explored was 0.005 $Å^{-1} \leq q \leq 0.23$ $Å^{-1}$, with counting times of between 10 min and 1 h. Measurements were also made at the Institut Laue Langevin, Grenoble, on the D22 instrument with incident wavelengths 8 Å and 14 Å with three sample-detector distances, 2 m, 6 m and 17 m, corresponding to an explored wave vector range 0.001 $Å^{-1} \leq q \leq 0.15$ $Å^{-1}$. The sample temperature during the experiment was maintained at 25° ± 0.1 °C.

The sample cell consisted of 1-mm thick quartz windows separated by a 1-mm thick spacer, sealed with a Viton O-ring. After radial averaging, corrections for incoherent background, detector response and cell window scattering were applied [3]. Calibration of the scattered neutron intensity was performed using the signal either from standard samples of silica aerogel or water [4,5].

Small-angle coherent X-ray scattering measurements

SAXS observations were made on the BM2 beamline at the ESRF, Grenoble, France (http://www.esrf.fr/exp_facilities/BM2/BM2.html) with an incident wavelength $\lambda = 1.5$ Å and resolution $\Delta\lambda/\lambda = 2 \times 10^{-4}$. The primary beam diameter was reduced by slits to 100 μm immediately after the focusing mirror and a 10-μm diaphragm was placed 10 m downstream just before the sample. A CCD detector was located 2.3 m beyond the sample. The spatially coherent beam thus obtained had a coherence area approximately equal to the detector pixel size, 22 μm. The beamstop was a gold cylinder of diameter 0.5 mm, glued to a thin Kapton foil. The evacuated flightpath between the mirror and the beamstop was free of windows.

Small-angle coherent light scattering measurements

Small-angle dynamic light scattering measurements were made with a 2-mW HeNe laser source. Light scattered from the sample was focused by a Fresnel lens on a CCD camera which collected successive images at a adjustable rate (ca. 1 s^{-1}) and then transferred them to a computer to calculate the intensity correlation function for each of the 512 x 512 pixels of the CCD. These correlation functions were grouped into subsets corresponding to different values of q, thus yielding simultaneous ensemble-averaged correlation functions for a wide range of q values [6].

Background

In a binary neutral gel system consisting of a polymer network and diluent, the scattering intensity can be described to a good approximation by the expression

$$I(q) = \Delta\rho^2 \left[\frac{kT\varphi^2}{M_{os}} \frac{1}{1+q^2\xi^2} + \frac{8\pi\Xi^3 \left\langle \delta\varphi^2 \right\rangle}{\left(1+q^2\Xi^2\right)^2} \right] \qquad (1)$$

where $\Delta\rho^2$ is the contrast factor between polymer and solvent. The first and second terms in the square brackets come respectively from the osmotic fluctuations and the static variations in concentration due to random elastic constraints. As the gel swells, the mean square static concentration fluctuation $<\delta\varphi^2>$ in the second term of Eq. 1 increases. This behavior is

illustrated in Fig. 1, where the scattering intensity $I(q)$ of a solution of uncrosslinked silicone sample is compared with that of the corresponding gel swollen to the same degree in the same solvent. Although the liquid-like feature near $q = 0.1$ Å^{-1} is clearly distinguishable in the gel, a strong increase in intensity dominates the low-q region of the gel spectrum, corresponding to the second term in Eq. 1.

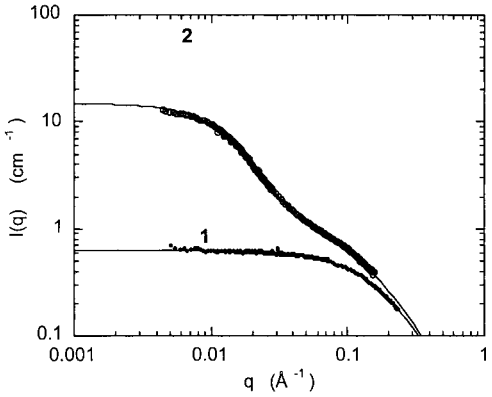

Figure 1. SANS spectra from a silicone solution in deuterated acetone (1), compared with that of a silicone gel swollen in the same solvent at the same volume fraction $\varphi = 0.33$ (2). The lines are fits of the solution data to the first term in Eq. 1 and of the gel data to the full Eq. 1.

The thermal correlation lengths ξ found from the fits to the data in Fig. 1 are 7 Å for the solution and 9 Å for the gel. When a filler is introduced into the polymer, the system becomes ternary (i.e. polymer, filler and solvent). The scattering response is then

$$I(q) = kT\,[(\rho_p - \rho_s)^2\, S_{pp}(q) + (\rho_p - \rho_s)(\rho_f - \rho_s)\, S_{pf}(q) + (\rho_f - \rho_s)^2\, S_{ff}(q)] \qquad (2)$$

where, ρ_p, ρ_f and ρ_s are the scattering length densities of the polymer, filler and solvent respectively. To solve for the three partial structure factors S_{pp}, S_{ff} and S_{pf}, which define the scattering from the polymer component, that from the filler and that of the interface between polymer and filler, respectively, $I(q)$ must be measured for at least three different values of the solvent scattering length ρ_s. This is achieved by swelling the sample to the same degree in a solvent containing different proportions of deuterated solvent in order to modify the scattering contrast of different components. Typical results of this procedure [7] are shown in Fig. 2, where the polymer partial structure factor $S_{pp}(q)$ is plotted for a filled crosslinked and a filled uncrosslinked PDMS system (sample 2) at approximately identical concentrations ($\varphi \approx$ 0.2). Both spectra exhibit a characteristic curvature at the lowest values of q, revealing the presence of objects having a radius close to 500 Å. This feature is associated with a polymer

shell that forms around the filler aggregates. This scattering region is followed at higher q by a steep drop in intensity with a slope of approximately –4, indicative of scattering from smooth polymer surfaces (Porod scattering) [8]. The area of these polymer surfaces may be estimated from the relation

$$\Sigma_p = \frac{kT}{2\pi} \lim_{q\to\infty} S_{pp}(q) q^4 \qquad (3)$$

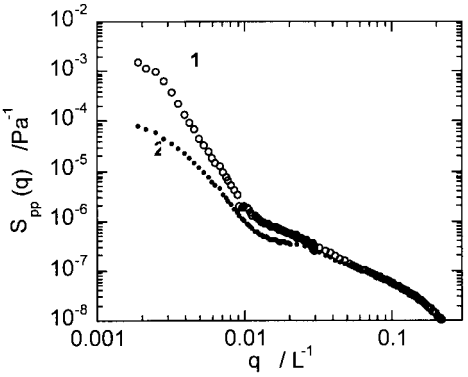

Figure 2. Polymer-polymer partial structure factors $S_{pp}(q)$ of a filled PDMS gel (1) and the corresponding filled uncrosslinked solution, sample 2 (2).

At intermediate values of q (0.01 Å^{-1} ≤ q ≤ 0.03 Å^{-1}), a shoulder is visible in the spectrum from the gel, caused by the elastic constraints imposed by the crosslinks, corresponding to the second term in Eq. 1. As expected, this feature is absent, or at least less pronounced than in the spectrum of the uncrosslinked solution. At the high q-end of the curves, a further drop in intensity can be observed, which is defined by the thermal correlation length of the osmotic fluctuations [1]. This behavior is described by the first term in Eq. 1, with $\xi \approx 15$ Å.

For the silica structure factor $S_{ff}(q)$ (not shown here), a Porod scattering regime with slope -4 is also observed, but only at the highest values of q. The specific surface area of these filler particles is then given by [8]

$$\frac{\Sigma_f}{Vd} = \frac{\pi}{d} \frac{\lim_{q\to\infty} S_{ff}(q) q^4}{\int S_{ff}(q) q^2 \, dq} \qquad (4)$$

where V is the scattering volume of the silica in the sample and d is its density.

Discussion

Figure 3 shows the partial structure factors found on applying the contrast variation technique to an uncrosslinked PDMS sample in which the silica filler particles have undergone a second, additional treatment with hexamethyldisilazane to improve the interaction with the surrounding polymer.

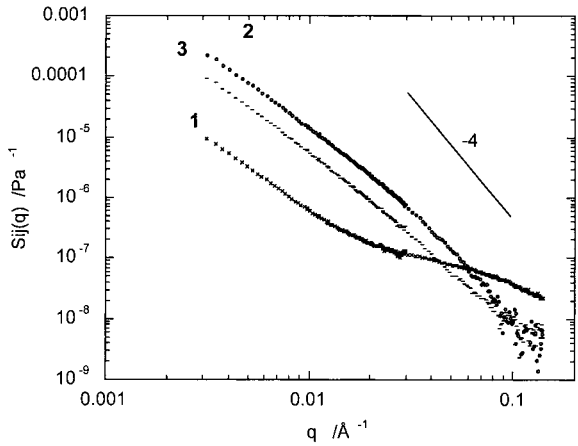

Figure 3. Partial structure factors $S_{pp}(q)$ (1), $S_{ff}(q)$ (2) and $S_{pf}(q)$ (3) in PDMS sample with hexamethyldisilazane-treated filler.

Comparison with the straight line of slope -4 in this figure allows to identify regions where Porod scattering prevails. This behavior shows up only for the silica structure factor at high values of q. The specific surface area determined from Eq. 4 for this sample is 300±30 m^2/g, in agreement with the results of independent BET surface area measurements.

For sample 2, the specific surface area of the silica is found to be 440 m^2/g. However, the ratio of the surface area of the polymer to that of the filler, Σ_p/Σ_f, (Eq. 3), is less than 0.02 in this sample. This surprising result shows that, when this filled system is swollen in toluene, polymer chains separate from the aggregate structures and form a smooth barrier at the outer edge. But in the sample containing the hexamethyldisilazane-treated filler, no equivalent smooth surface is visible in the polymer structure factor, indicating that the coupling agent prevents separation of the polymer from the filler. As shown in Fig. 4, $S_{pp}(q)$ can be fitted to an expression similar to Eq. 1, but where the exponent of the second term is smaller than 2:

$$I(q) = (\rho_p - \rho_s)^2 \left[\frac{kT\varphi^2}{M_{os}} \frac{1}{1+q^2\xi^2} + \frac{A}{(1+q^2\Xi^2)^{3/2}} \right] \qquad (5)$$

Equation 5 is the result expected for star polymers [9] in a semidilute polymer solution. This finding implies that polymer chains do not form a distinct outer sheath around silica aggregates but penetrate inside and adhere to the surface. In this case, since the Porod scattering region for the polymer is not clearly distinguishable from the intensity scattered by thermal fluctuations, it is not easy to evaluate quantitatively the area of polymer in direct contact with the solid.

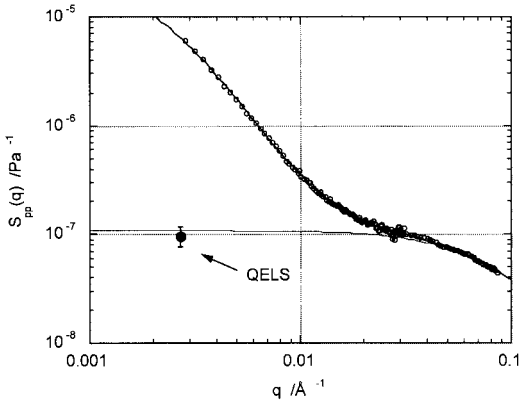

Figure 4. Partial structure factor $S_{pp}(q)$ from Fig. 3 showing fit of Eq. 5 (line) together with the osmotic component (first term in Eq. 5) and the osmotic susceptibility measured from dynamic light scattering (filled circle).

Figure 4 also shows the term arising from osmotic concentration fluctuations (first term in Eq. 5) resulting from the fit of Eq. 5 to the data. The amplitude of this term can also be determined independently by dynamic light scattering [10]. The result of this measurement, shown as a filled circle in Fig. 4, lies on the horizontal plateau of the dynamic component. This agreement lends credibility to the physical model on which the data analysis is based, and illustrates the consistency between the neutron and light scattering results.

Coherent X-ray scattering spectroscopy was used to probe the dynamics of structural relaxation processes in the filled PDMS samples, in the absence of solvent [11,12]. This technique, which is identical in concept to visible dynamic light scattering spectroscopy, relies on a synchrotron source for the X-rays. The intensity correlation that is measured is given by [13]:

$$G(t) = \langle I(q,0)I(q,t)\rangle / \langle I(q,t)\rangle^2 = 1 + \beta \exp(-2\Gamma t) \qquad (6)$$

where $I(q,t)$ is the intensity of a speckle at wave vector q and time t. The factor β is an instrumental constant and

$$\Gamma = Dq^2 \qquad (7)$$

is the characteristic relaxation rate of light scattered by particles having a diffusion coefficient D. The use of X-rays permits the study of relaxation processes at values of q beyond the range accessible to visible light scattering and provides a unique means of investigating the dynamics of structural rearrangements at high resolution.

In the present system, structural relaxation occurs when the samples are mechanically stirred. After the initial blending process, the silica aggregates in the polymer melt cluster into

loose larger units called agglomerates. These associations can be disrupted by stirring, but immediately afterwards they start to reform. It is therefore expected that the observed diffusion rate of the particle in suspension will be higher immediately after stirring but the relaxation rate will subsequently decrease as the agglomerates reform. To account for this process, we set

$$\Gamma = Dq^2 [1+a \exp(-t_0/\tau_s)] \qquad (8)$$

where D is the diffusion coefficient of the agglomerates and the factor $(1+a)$ describes the increase in diffusion rate due to the fragmentation into aggregates. In Eq. 8, t_0 is the time lapse between the mechanical perturbation and the measurement and τ_s is the structural relaxation time.

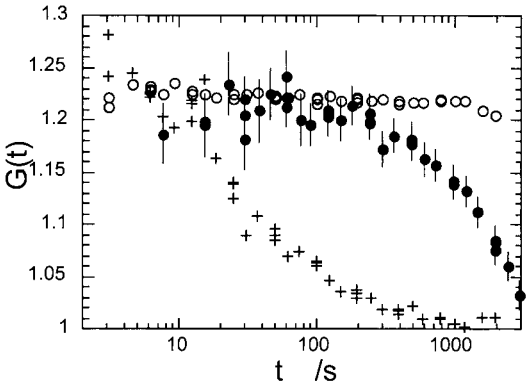

Figure 5. Coherent X-ray correlation functions $G(t)$ measured for dry aerosol powder (open circles), untreated silica dispersed in neat PDMS (+) and neat sample 2 (filled circles).

Figure 5 shows the intensity correlation functions obtained with coherent X-rays for $q = 2\text{x}10^{-3}$ Å^{-1} from three different samples. For correlator delay times t greater than one hour, the correlation function of a dry aerosol powder displays no relaxation, as is expected from a system that is completely frozen. For the two silica suspensions in PDMS, however, relaxation is clearly visible: the suspension of the untreated fumed silica relaxes in about 100 s, while the uncrosslinked sample 2 displays a much slower relaxation.

Figure 6 compares the relaxation behavior of sample 1 (as a function of q) for the data obtained both from coherent X-ray scattering and from small-angle light scattering.

In this representation, each data set approaches the same limiting curve with slope 2, corresponding to Eq. 7 in which $D = 4.6 \times 10^{-14}$ cm^{2}s^{-1} is the diffusion coefficient of large agglomerates.

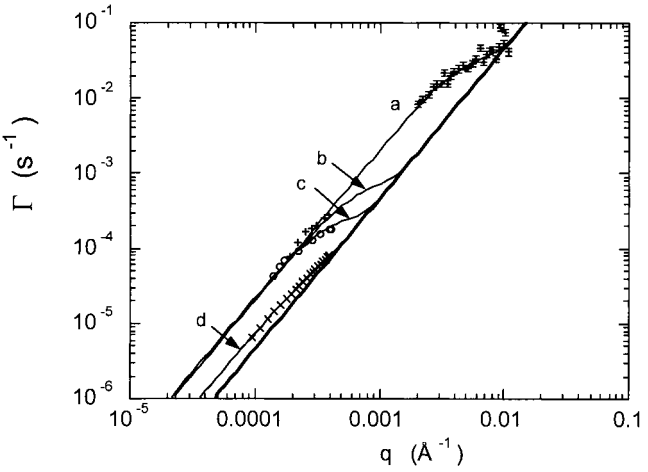

Figure 6. Relaxation rates $\Gamma(q)$ measured for sample 1. The thick straight line is defined by Eq. 7 where $D = 4.6 \times 10^{-14}$ cm^{2}s^{-1}. The upper set of data is from coherent X-ray spectroscopy with time lapse $t_0 = 3000$ s after stirring, the lower data sets are from small-angle dynamic light scattering with $t_0 = 10^5$ s , 3×10^5 s and 10^6 s, respectively. Thin lines are calculated from Eqs. 8 and 9 with $D_s = 1 \times 10^{-15}$ cm^{2}s^{-1}.

The thin lines drawn through the data sets are obtained from Eq. 8 for the measured time lapses t_0 = 3000 s, 10^5 s, 3×10^5 s and 10^6 s. To yield a consistent description of the experimental observations, the structural relaxation rate must obey a relation of the form

$$1/\tau_s = D_s q^2. \qquad (9)$$

where $D_s = 10^{-15}$ cm^{2}s^{-1}. This result shows that over the whole investigated q range, the structural relaxation process is diffusion-controlled.

Conclusions

It is demonstrated that small-angle neutron scattering and contrast variation allow to make structural characterization of filled polymer systems. In this study, differences are highlighted between the structure of polymers containing fumed silica with different surface properties. It is found that the distribution of the polymer is perturbed in the vicinity of solid surfaces. Swelling these rubbers and estimation of the surface area of the filler and the surface coverage of the polymer reveals further structural details. In the case of weak interactions, the solvent causes the polymer to desorb almost completely from the filler particles. However, in fillers treated with coupling agents, thorough penetration of the polymer into the filler structure is observed.

It is shown that coherent X-ray scattering is a powerful method for investigating the relaxation processes in filled polymers. It is found that structural relaxation following an external mechanical perturbation proceeds by a diffusion-controlled mechanism.

Acknowledgements

The authors acknowledge the support of the National Institute of Standards and Technology, U.S. Department of Commerce, the Institut Laue-Langevin, Grenoble and the European Synchrotron Radiation Facility, Grenoble, France, in providing access to the small-angle neutron scattering instruments NG3 and D11 and to the small-angle X-ray instrument at BM2. We are grateful to Drs B. Hammouda and J.F. Bérar for their invaluable help in these measurements. This work is partly based upon activities supported by the National Science Foundation under agreement No. DMR-9423101.

1. P.G. de Gennes, Scaling Concepts in Polymer Physics, Cornell, Ithaca 1979.
2. J.S. Higgins and H.C. Benoît, Polymers and Neutron Scattering, Oxford Science Publications, Oxford, 1994.
3. A Computing Guide for Small Angle Neutron Scattering Experiments, R.E. Ghosh, S.U. Egelhaaf, A.R. Rennie, Institut Laue Langevin, June 2000.
4. NIST Cold Neutron Research Facility, NG3 and NG7 30 meter SANS Instruments Data Acquisition Manual, January 1999.
5. P. Lindner, F. Leclercq and P. Damay, Physica B, **291**, 152 (2000).
6. L. Cipelletti and D.A. Weitz, Rev. Sci. Instrum. **70**, 3214 (1999).
7. A.M. Hecht, E. Geissler and F. Horkay, Phys. Rev. E **59**, 1976 (1999).
8. G. Porod in Small Angle X-ray Scattering (O. Glatter and O. Kratky, Eds), Academic Press 1985.
9. G.S. Grest, K. Kremer and T.A. Witten, Macromolecules **20**, 1376 (1987).
10. F. Horkay, W. Burchard, E. Geissler and A.M. Hecht, Macromolecules **26**, 1296 (1993).
11. M. Sutton, S.E. Nagler, S.G.J. Mochrie, T. Greytak, L.E. Bermann, G. Held and G.B. Stephenson, Nature **352**, 608 (1991).
12. E. Geissler, A.-M. Hecht, C. Rochas, F. Bley, F. Livet and M. Sutton, Phys. Rev. E **62**, 8308 (2000).
13. B.J. Berne and R. Pecora, Dynamic Light Scattering, Wiley, New York 1976.